A study of substitutional disorder in Cr^{3+} : $CaYAlO_4$: II. Electron spin resonance and polarization of optical spectra

1996 J. Phys.: Condens. Matter 8 10633

(http://iopscience.iop.org/0953-8984/8/49/048)

J. Phys.: Condens. Matter **8** (1996) 10633–10646. Printed in the UK

A study of substitutional disorder in Cr^{3+}:$CaYAlO_4$: II. Electron spin resonance and polarization of optical spectra

M Yamaga†, T Yosida‡, M Fukui‡, H Takeuchi§, N Kodama‖+, Y Inoue‖, B Henderson¶, K Holliday¶ and P I Macfarlane¶

† Department of Physics, Gifu University, Gifu 501-11, Japan
‡ Nakanihon Automotive College, Sakahogi, Kamo 505, Japan
§ Department of Electronics and Information, Nagoya University, Nagoya 464-01, Japan
‖ Tosoh Corporation, Hayakawa, Ayase 252, Japan
¶ Department of Physics and Applied Physics, University of Strathclyde, Glasgow G1 1XN, UK

Received 24 June 1996

Abstract. Electron spin-resonance (ESR) studies of Cr^{3+} in $CaYAlO_4$ (CYA) reveal spectra consisting of fine-structure pairs of narrow symmetric lines and fairly broad asymmetric lines, corresponding to Cr^{3+} ions in sites with ordered and disordered configurations of the second-nearest-neighbour Ca^{2+}/Y^{3+} ions, respectively. The polarized intensities of the $^4A_2 \to {}^4T_2$ absorption band and the R_1-line fluorescence, measured with the E-vector of the radiation parallel (I_π) and perpendicular (I_σ) to the c-axis, are in the ratio $I_\pi{:}I_\sigma \simeq 3{:}1$. These polarization ratios suggest that the CrO_6^{9-} octahedra undergo an angular distortion such that the magnetic ζ-axis of the spectrum is rotated away from the crystal c-axis. The microstructure of the Cr^{3+} surrounding is discussed in terms of the ESR and polarization results.

1. Introduction

In paper I [1], we discussed the inhomogeneous broadening of the R_1-line fluorescence of Cr^{3+} ions in $CaYAlO_4$ (CYA) caused by *substitutional disorder* of the Ca^{2+}/Y^{3+} sites on the basis of fluorescence-line-narrowing (FLN) studies. The inhomogeneous broadening is assigned to variations of the crystal field at the Cr^{3+} sites. Estimates of the distributions of the octahedral and non-octahedral contributions to the crystal field were made from the results of the resonantly excited and non-resonantly excited FLN spectra. These estimates show that the distribution of the non-octahedral component to the crystal field makes the dominant contribution to the inhomogeneous broadening. The non-octahedral components represent the extent to which there are deviations from cubic symmetry to lower symmetry. Electron-spin-resonance (ESR) studies may determine the sources of distortions causing the inhomogeneous broadening on a microstructural scale, recognizing the distinct contributions from the first- and second-nearest-neighbour ions of the central Cr^{3+} ion. The polarization of the optical spectra strongly reflects the symmetries of the ground and excited states, and may be interpreted in terms of the effects of odd-parity distortions [2]. This paper reports the results of our studies of the ESR and polarized optical spectra of Cr^{3+} in CYA. On the basis of these measurements a model of the microstructure of the environments of Cr^{3+} ions in the disordered host crystal is proposed.

+ Present address: Department of Chemistry, Faculty of Education, Akita University, Akita 010, Japan.

0953-8984/96/4910633+14\$19.50

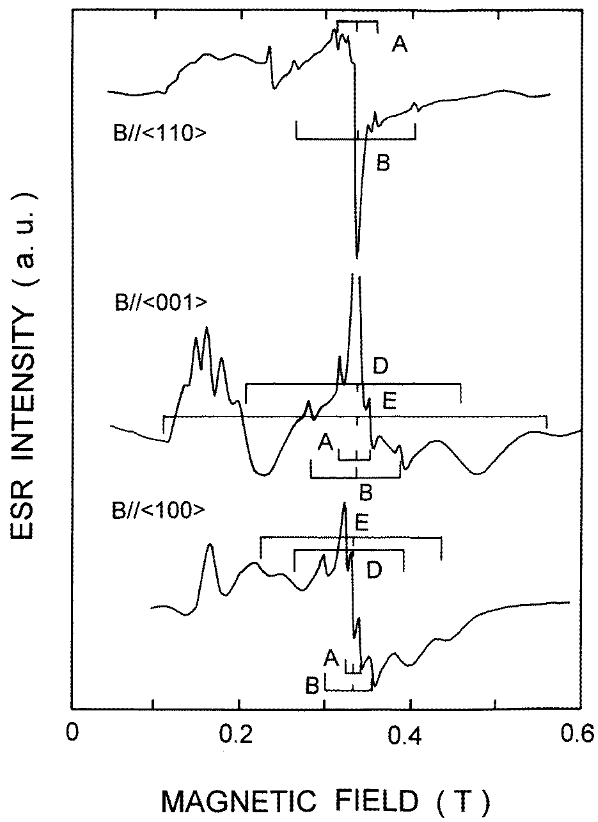

Figure 1. X-band ESR spectra of Cr^{3+} in CYA measured at 300 K and with $\boldsymbol{B} \parallel \langle 100\rangle$, $\langle 001\rangle$, and $\langle 110\rangle$.

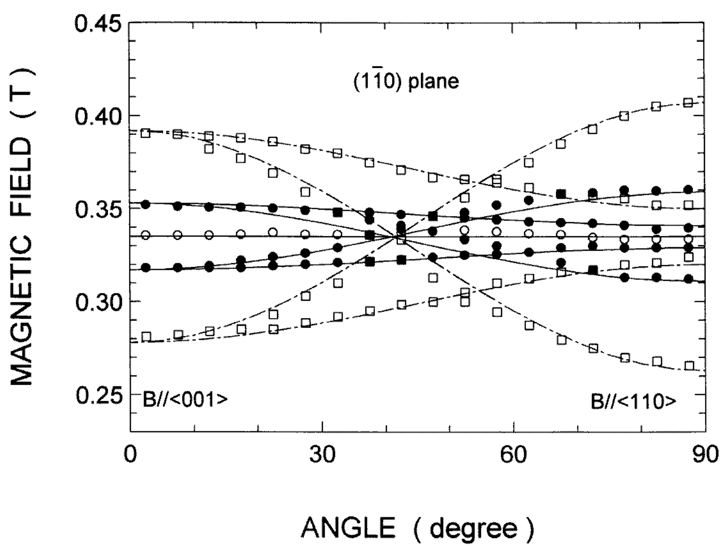

(a)

Figure 2. See facing page.

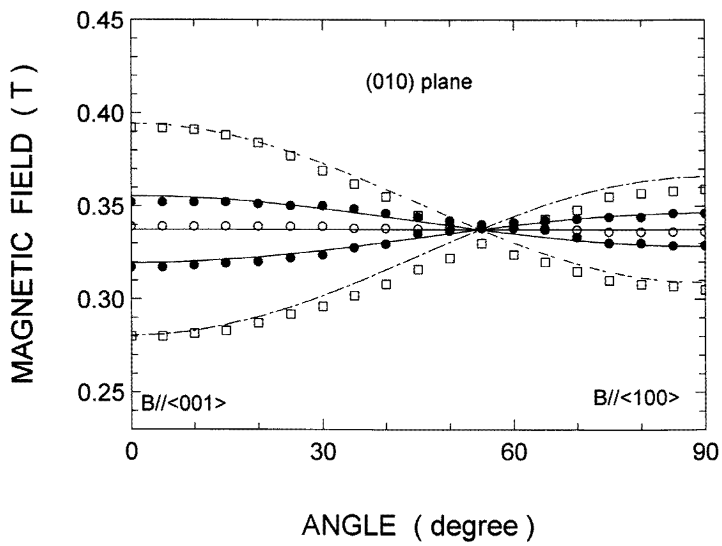

(b)

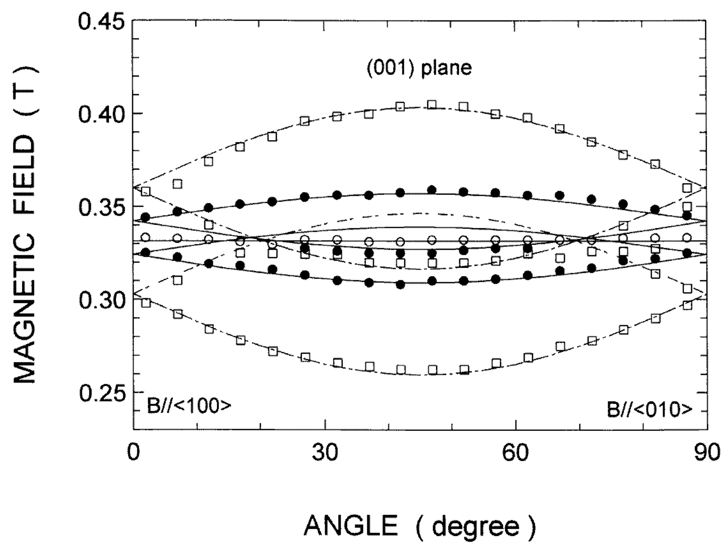

(c)

Figure 2. Angular variations of the A and B lines of Cr^{3+} in CYA with magnetic fields applied in (a) the $(1\bar{1}0)$, (b) the (010) and (c) the (001) planes. The solid and chain curves were calculated using equation (1) and the spin-Hamiltonian parameters in table 1.

2. Experimental procedure

The details of the crystal structure and the crystal growth of CYA were described in paper I [1]. Cr^{3+} impurities substitute preferentially for Al^{3+} ions in this crystal [3]. The concentration of Cr^{3+} ions in the crystals is 0.1 at.%. The as-grown crystals were cut and polished into samples with approximate dimensions $1.5 \times 1.5 \times 2$ mm^3 for ESR study or $4 \times 4 \times 4$ mm^3 for optical measurements, the cut faces being normal to the *a*-, *b*-, and *c*-axes of the crystal.

ESR measurements were made at temperatures in the ranges 1.6–4.2 K, 4.2–70 K, and 77–300 K. A Q-band ($\nu \sim 35$ GHz) ESR spectrometer using 100 kHz field modulation was used, and an X-band ($\nu \sim 9.2$ GHz) ESR spectrometer using 270 Hz and 100 kHz field modulation was used. Optical absorption spectra were measured at room temperature using a dual-beam spectrophotometer. The polarization was measured by inserting a Glan–Thompson prism in the sample beam of the spectrophotometer and rotating it. Measurements of the fluorescence spectrum of Cr^{3+} in CYA were made on samples mounted on a cold finger in a cryorefrigerator at a working temperature in the range 10–300 K. Fluorescence was excited using the 488 nm line from a cw Ar^+-ion laser, the excitation beam being mechanically chopped at a frequency of 800 Hz. Fluorescence from the sample was focused onto the entrance slit of a 1/4 m monochromator and detected at the exit slit by a Hamamatsu Photonics R943-02 photomultiplier, amplified by a Keithley 428 current amplifier, and measured by a Stanford Research Systems SR250 boxcar averager. The polarization of the fluorescence was measured using a linear polarizer.

Table 1. Spin-Hamiltonian parameters for Cr^{3+} in $CaYAlO_4$.

Line	A	B	C	D	E
$g_\xi \approx g_\eta \approx g_\zeta$	1.98 ± 0.01	1.98 ± 0.01	1.98 ± 0.01	1.98 ± 0.01	1.98 ± 0.01
b_2^0 (10^{-4} cm^{-1})	110 ± 10	330 ± 20	20 ± 5	650 ± 100	1300 ± 200
b_2^2 (10^{-4} cm^{-1})	-55 ± 5	-200 ± 20	-10 ± 5	-300 ± 50	-1100 ± 300

3. Experimental results

3.1. ESR results

Figure 1 shows the X-band ESR spectra at room temperature with the static magnetic field $\boldsymbol{B} \parallel \langle 110\rangle$, $\langle 001\rangle$ and $\langle 100\rangle$ crystal axes and at a microwave frequency of 9.189 GHz for the Cr:CYA sample. The spectra consist of narrow lines and fairly broad lines: with the static field $\boldsymbol{B} \parallel \langle 001\rangle$ the widths of the narrow and broad lines are ∼50 G and ∼450 G, respectively. The spectra are asymmetric about ≃0.33 T, there being pairs of fine-structure transitions, $\Delta M_S = \pm 1$ with $M_S \pm 1/2 \leftrightarrow \pm 3/2$ denoted by A, B, D and E centred on the $M_S - 1/2 \leftrightarrow +1/2$ transition. The broad lines at around 0.18 T are due to the forbidden $\Delta M_S = \pm 2$ transitions of the Cr^{3+} spin sublevels.

Figure 2 shows the angular dependence of the sharp resonance lines A and B for the Cr:CYA sample observed at 300 K as the magnetic field is rotated in the $(1\bar{1}0)$, (010), and (001) planes. The resonance field positions of the A and B lines are denoted by the solid circles and squares, respectively. The isotropic lines at 0.337 T due to $-1/2 \leftrightarrow +1/2$ transitions of the A and B lines are denoted by open circles. These angular dependences of the narrow lines shown in figure 2 are fitted to a spin Hamiltonian with orthorhombic symmetry [4, 5]:

$$\mathcal{H} = \mu_B (g_\xi S_\xi B_\xi + g_\eta S_\eta B_\eta + g_\zeta S_\zeta B_\zeta) + \frac{1}{3}(b_2^0 O_2^0 + b_2^2 O_2^2) \quad (1)$$

where S is 3/2, μ_B is the Bohr magneton and O_n^m are the Stevens operators. The principal ζ-axis of the spectrum is defined as that magnetic field direction at which the fine-structure

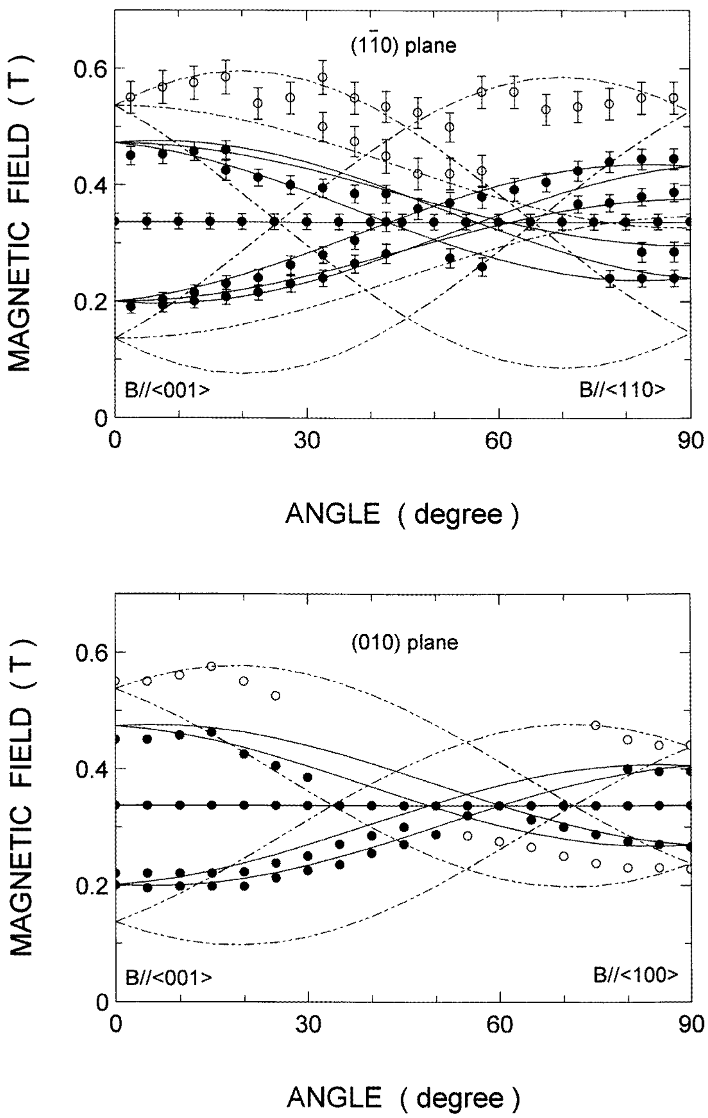

Figure 3. Angular variations of the D and E lines of Cr^{3+} in CYA with magnetic fields applied in the (010) and (1$\bar{1}$0) planes. The solid and chain curves were calculated using equation (1) and the spin-Hamiltonian parameters in table 1.

splitting is maximum, i.e. when $\boldsymbol{B} \parallel \langle 110\rangle$. The three principal axes ξ, η and ζ of the A and B lines are parallel to the $\langle 001\rangle$, $\langle 1\bar{1}0\rangle$ and $\langle 110\rangle$ in figure 1, respectively. The chain and solid curves in figure 2, calculated using equation (1) with the spin-Hamiltonian parameters listed in table 1, fit the observed angular variations of the A and B lines, respectively, very well. Figure 3 shows the orientation dependence of the broad lines D and E in the (1$\bar{1}$0) and (010) planes. The lines are too broad to assign to specific transitions when the magnetic field is rotated away from the crystal axis. The angular variations show that the principal ζ-axes for lines D and E are tilted by $\sim 7^\circ$ and $\sim 20^\circ$ from the $\langle 001\rangle$ direction towards the

⟨111⟩ direction, respectively. The rough estimates of the fine splittings, b_2^0 and b_2^2 for lines D and E, are given in table 1.

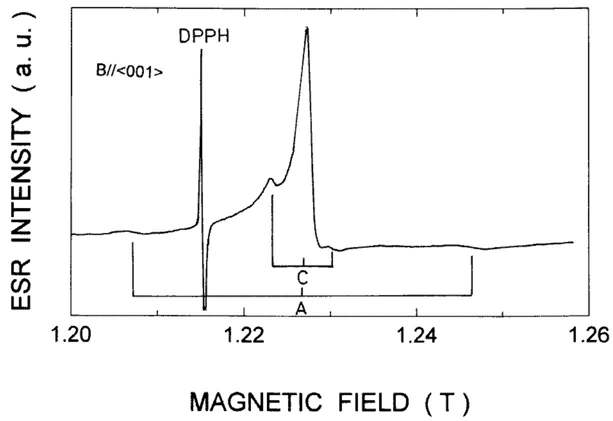

Figure 4. Q-band ESR spectra of Cr^{3+} in CYA with $\boldsymbol{B} \parallel \langle 001\rangle$ at 300 K.

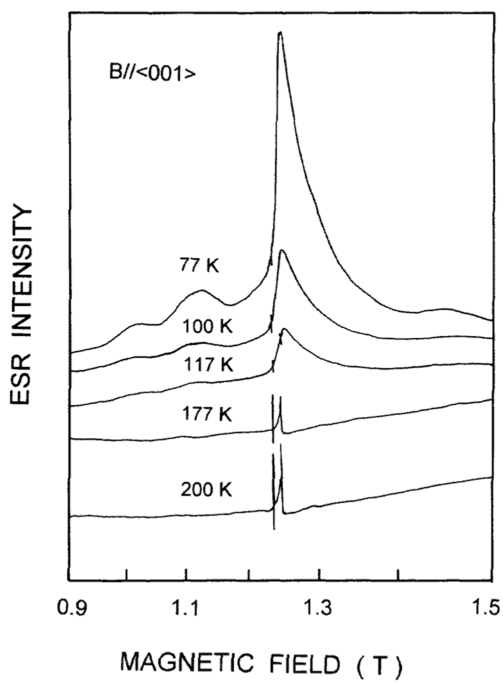

Figure 5. The temperature dependence of the Q-band ESR spectra of Cr^{3+} in CYA with $\boldsymbol{B} \parallel \langle 001\rangle$.

The Q-band spectrum in figure 4 measured at room temperature with $\boldsymbol{B} \parallel \langle 001\rangle$ reveals a further pair of narrow lines, denoted by C, which is not resolved at X band. The small fine-structure splitting of this spectrum shows that the symmetry of this Cr^{3+} centre is close to octahedral. The pattern of the angular variation of the C line in the (010) plane is similar to those of the A and B lines observed at X band as shown in figure 2(b). Although the C line is observed only for the magnetic field applied in a direction near to the ⟨100⟩ direction in the (001) plane, the fine splitting increases slightly when the field is off the ⟨100⟩ axis. These results suggest that the principal ζ-axis of the C line is parallel to the ⟨110⟩ axis. The spin-Hamiltonian parameters are summarized in table 1.

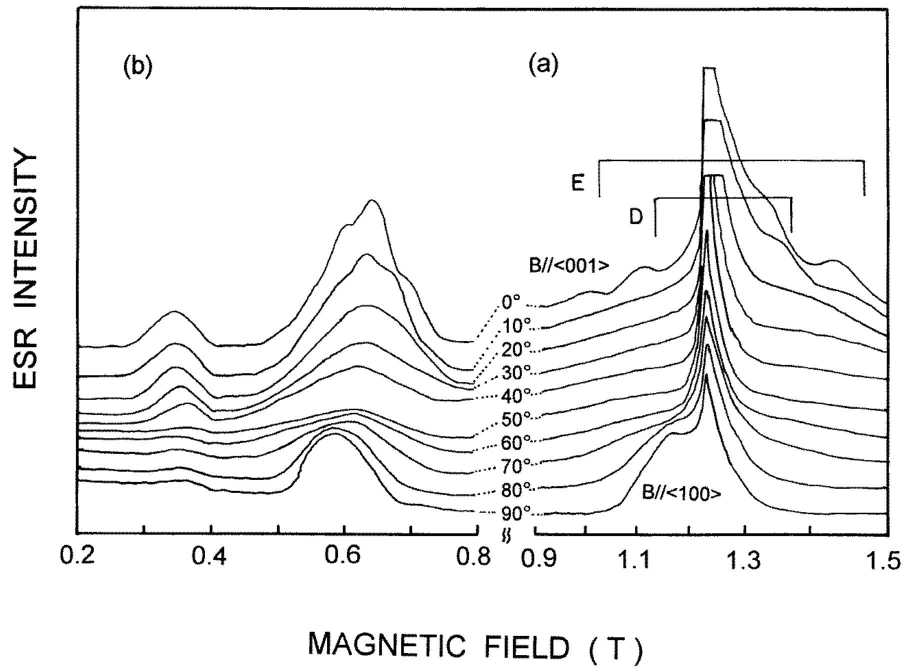

Figure 6. Angular variations of ESR spectra of Cr^{3+} in CYA with magnetic fields in the (010) plane at 1.6 K: (a) allowed transitions and (b) forbidden transitions.

As the temperature is decreased down to ~120 K, intense and strongly asymmetric lines appear at $B \sim 1.25$ T as shown in figure 5. These broad lines are coincident with the D and E lines of the X-band spectra. The asymmetry of the ESR spectrum is due to the long spin–lattice relaxation time. These broad lines are wide because of the distributions of the fine-structure splittings and/or of the directions of the principal axes which result from the *substitutional disorder* on the Ca^{2+}/Y^{3+} sites in CYA as pointed out in paper I [1]. Such broad lines are not observed for multiple-quantum transitions of Cr^{3+} ions in crystals of MgO or Al_2O_3. The shapes of the lines in the Q-band spectrum did not change as the temperature decreased from 77 K to 1.6 K. The orientation dependence of the Q-band spectrum measured at 1.6 K with magnetic fields in the (010) plane is shown in figure 6. The intense asymmetric line at 1.25 T with $\boldsymbol{B} \parallel \langle 001 \rangle$ is accompanied by a pair of similarly broad fine-structure lines. When the magnetic field is rotated from the ⟨001⟩ direction towards the ⟨100⟩ direction, these fine-structured lines split into two broader branches where the resonances could not be resolved at all. The asymmetric and broad lines that are apparent for $\boldsymbol{B} \parallel \langle 100 \rangle$ occur because of magnetically equivalent sites. The weak signals in figure 6(b) that are observed at close to one third and one half of the field ($B \sim 1.25$ T) of the asymmetric and intense line are assigned to the forbidden transitions

($\Delta M_S = 3, 2$) as in the X-band spectra. It is difficult to estimate the spin-Hamiltonian parameters using the experimental data in figure 6 with equation (1) because of the width and asymmetry of the ESR spectra. The widths of the fairly broad lines at $B \sim 1.25$ T and the forbidden-transition lines at $B \sim 0.35$ T and $B \sim 0.6$ T for any direction of the magnetic field can be reproduced using the spin-Hamiltonian parameters in table 1 obtained from the D and E lines measured by the X-band spectrometer.

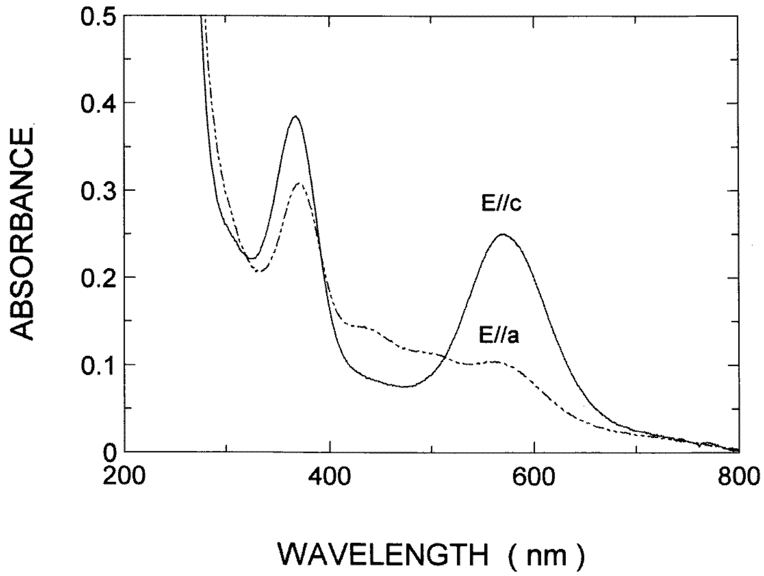

Figure 7. The polarization of the absorption spectra of Cr^{3+} in CYA measured at 300 K. The orientation in which for π- and σ-polarizations the E-vector of the radiation is parallel and perpendicular to the c-axis, respectively, is assumed.

3.2. Polarization of optical spectra

The optical absorption spectrum of the Cr:CYA sample shown in figure 7 has strong absorption bands with peaks at 368 nm and 566 nm at 300 K due to the $^4A_2 \rightarrow {}^4T_1$ and $^4A_2 \rightarrow {}^4T_2$ transitions, respectively. There are additional weak peaks near 430 nm and 500 nm. This spectrum is strongly polarized, the peaks at 368 nm and 566 nm being much stronger when the E-vector of the radiation is along the c-axis ($\boldsymbol{E} \parallel \langle 001 \rangle$) than when it is along the a- and b-axes ($\boldsymbol{E} \parallel \langle 100 \rangle$, $\langle 010 \rangle$). The band with a peak at 430 nm is strongly polarized along the a-axis and the intensity ($\boldsymbol{E} \parallel \boldsymbol{c}$) is negligibly weak compared with the background intensity.

The fluorescence excited in the $^4A_2 \rightarrow {}^4T_2$ absorption band consists of the Cr^{3+} R lines and accompanying phonon side bands at temperatures in the range 10–300 K. The polarized R_1-line spectra with the E-vector along the c- and a-axes and measured at 10 K are shown in figure 8. The fluorescence intensity with $\boldsymbol{E}_{em} \parallel \boldsymbol{c}$ is about three times larger than those measured with $\boldsymbol{E}_{em} \parallel \boldsymbol{a}$. This polarization ratio is nearly equal to that of the $^4A_2 \rightarrow {}^4T_2$ absorption band.

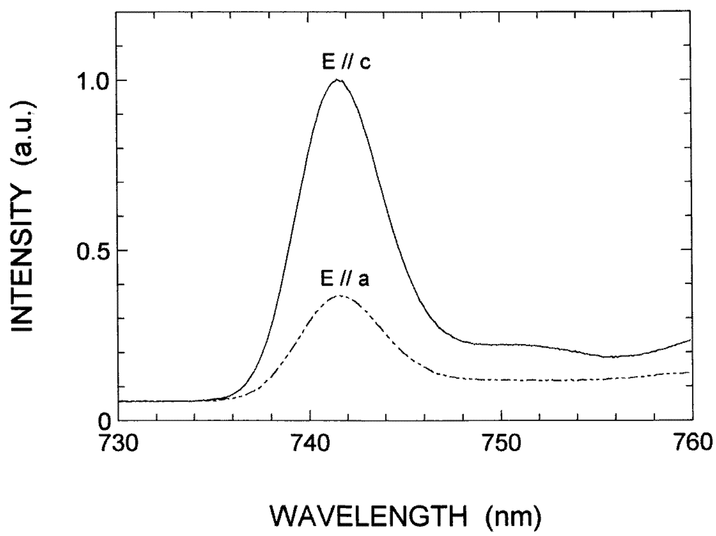

Figure 8. The polarization of the R_1-line fluorescence of Cr^{3+} in CYA excited by the 488.0 nm laser line and measured at 10 K.

4. Discussion

The R_1-line fluorescence shows a large inhomogeneous width, the origin of which is the random distribution of Ca^{2+} and Y^{3+} ions such that the Ca^{2+}/Y^{3+} composition ratio of 1:1 is maintained in the disordered host lattice [1]. The CrO_6^{9-} octahedron is strongly perturbed by the second-nearest-neighbouring Ca^{2+} and Y^{3+} ions. Here we discuss the microstructure of the Cr^{3+} environment in CYA implied by the ESR and optical polarization results.

4.1. The local symmetry of Cr^{3+}

The ESR spectra observed at room and low temperatures are quite different. They show various distinguishable Cr^{3+} sites in the CYA crystal structure. The narrow A and B lines in figure 1 indicate that the principal ξ-, η-, and ζ-axes for both lines are parallel to the $\langle 001\rangle$, $\langle 1\bar{1}0\rangle$, and $\langle 110\rangle$ crystal directions, respectively, and that the intensity ratio is $I_A{:}I_B \simeq 2{:}1$. The narrow C lines in figure 4 are due to a centre with almost octahedral symmetry as implied by the small value of b_2^0. These narrow spectra are assigned to Cr^{3+} ions occupying sites that have an ordered configuration of second-nearest-neighbour Ca^{2+}/Y^{3+} ions. The broader spectra D and E observed mainly at low temperatures in X- and Q-band experiments correspond to Cr^{3+} ions at sites in which the Ca^{2+} and Y^{3+} ions replace each other on their respective sublattices, to yield many geometrically inequivalent sites. The effects of these variations in local configurations cause the inhomogeneous broadening of the ESR lines.

First, consider an ordered configuration of the Cr^{3+} complex containing four Ca^{2+} and four Y^{3+} ions in the second-nearest-neighbour sites as in figure 9(a). The Ca^{2+} and Y^{3+} ions each form interpenetrating tetrahedra with respect to each other. If we include the further third-nearest-neighbour Ca^{2+} and Y^{3+} ions along the c-axis, we obtain the three configurations denoted by **a**, **b**, and **c** in figure 9(a). The **a** complex is essentially ordered because the balance of charge in the complex is conserved. The AlO_6^{9-} octahedron in CYA as determined by x-ray diffraction is elongated along the c-axis, resulting in tetragonal

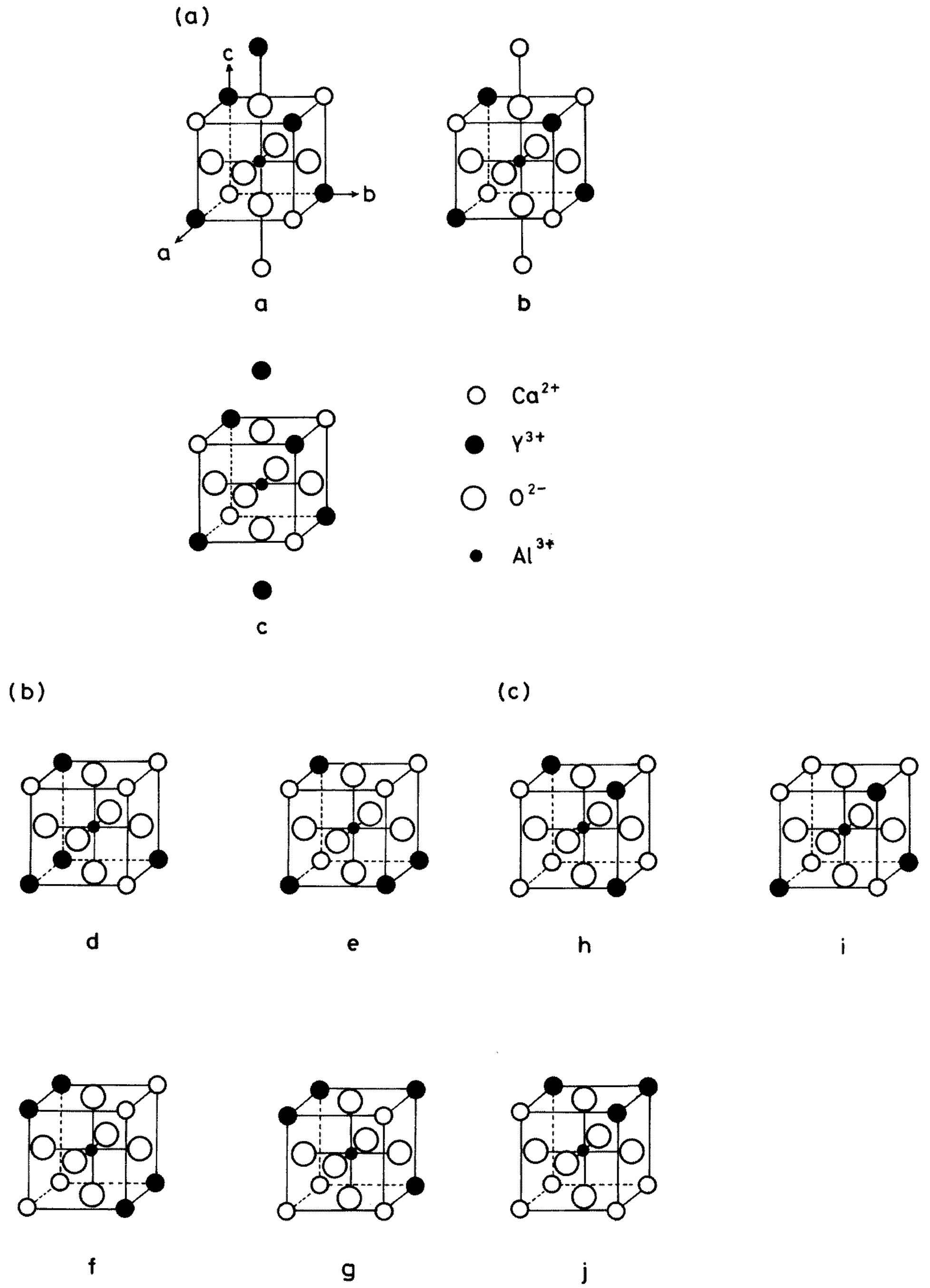

Figure 9. A model of Cr^{3+} complexes: (a) ordered configurations; (b), (c) disordered configurations.

symmetry. When one of the third-nearest-neighbouring Ca^{2+} and Y^{3+} ions on the *c*-axis is replaced by a different cation (the **b** and **c** complexes in figure 9(a)), the octahedra retain tetragonal symmetry along the c-axis, but the values of the fine-structure splitting, b_2^0, are enhanced or reduced relative to that of the **a** complex. The probability ratio of the **a**, **b** and **c** complexes is found to be 2:1:1, in agreement with the observation of three pairs of ESR lines (A, B and C lines) with this intensity ratio. The **a**, **b** and **c** complexes are expected to have tetragonal symmetry with the principal ζ-axis being parallel to the c-axis, an expectation inconsistent with the observation that the principal ζ-axis is parallel to $\langle 110 \rangle$ rather than the c-axis. In order to explain this discrepancy, we consider a model of other Cr^{3+} centres.

There are two other ordered configurations (not shown) containing four Ca^{2+} and four Y^{3+} ions: in one configuration four Ca^{2+} or four Y^{3+} ions occupy one of the separate parallel planes perpendicular to the a-, b-, and c-axes, each case resulting in tetragonal symmetry; in the other configuration two Ca^{2+} ions each occupy two parallel diagonal lines in separate planes, giving rise to an axial crystal field along the $\langle 110 \rangle$ direction. The former complex is physically unrealistic because of the charge imbalance. Although the latter complex can explain the ESR result, the question of why the most probable **a** complex does not exist in the disordered crystal remains. There is another possibility, that, for example, Al^{3+} vacancies produce an axial field along the $\langle 110 \rangle$ direction. However, there is the problem that Cr^{3+} ions are substituted near to Al^{3+} vacancies. It is difficult to clarify the origin of the principal ζ-axis parallel to the $\langle 110 \rangle$ direction.

Next, consider the two broad D and E spectra associated with Cr^{3+} ions in sites with random occupations of the second-nearest-neighbouring Ca^{2+}/Y^{3+} cation positions. There are four distinguishable disordered configurations shown in figure 9(b) each containing four Ca^{2+} and four Y^{3+} ions. The numbers of the equivalent sites for the **d**, **e**, **f**, and **g** complexes in figure 9(b) are 24, 24, 8 and 6, respectively. The principal axes of the **d** and **e** complexes are expected to be tilted away from the $\langle 001 \rangle$ direction towards $\langle 111 \rangle$ or $\langle 1\bar{1}1 \rangle$, the difference between the two complexes being in their angular tilts. On the other hand, the principal ζ-axis of the **f** complex is parallel to $\langle 0\bar{1}1 \rangle$, and that of the g complex is tilted away from $\langle 001 \rangle$. A final set of disordered configurations involving three Ca^{2+} and five Y^{3+} ions or alternatively five Ca^{2+} and three Y^{3+} ions is shown in figure 9(c). There are three distinguishable configurations denoted by **h**, **i** and **j**, for which there are 24, 8, and 24 equivalent sites, respectively. The probability that the **j** complex arises in a real crystal is very small because of the strongly polarized charge distribution.

It is now appropriate to decide which of the disordered complexes in figures 9(b) and 9(c) refer to the D and E ESR spectra which have their principal ζ-axes of the orthorhombically distorted octahedra tilted by $\sim 7^\circ$ and $\sim 20^\circ$ from the $\langle 001 \rangle$ direction towards $\langle 111 \rangle$, respectively. The disordered configurations in figure 9(b) contain two dominant, distinct **d** and **e** complexes which are tilted away from the $\langle 001 \rangle$ direction, as is the situation also for the complexes shown in figure 9(c). Assuming that the two distinguishable ESR spectra D and E, observed readily at low temperature, correspond to the disordered configurations, and that the most probable disordered configurations maintain charge neutrality—that is, four Ca^{2+} and four Y^{3+} ions—it seems more physically realistic that the **d** and **e** complexes in figure 9(b) are more probably linked to the D and E spectra than are the **h** and **i** complexes in figure 9(c). However, there is no other experimental evidence which supports the above assumption. If there is a reasonable probability that there exist three Ca^{2+} and five Y^{3+} ions or alternatively five Ca^{2+} and three Y^{3+} ions as the second-nearest-neighbour cation ions of the Cr^{3+} octahedron in CYA crystals, the above-proposed model should be changed.

The magnitudes of the g-factor and fine-structure parameters of Cr^{3+} in, for example, orthorhombic or monoclinic symmetry sites are related to the energy splitting of the $^4T_2$

excited state. The g-shift is proportional to $8\lambda/\Delta_i$ ($i = 0, \pm 1$), where λ is the effective spin–orbit parameter, and the Δ_i are the energy separations of the three $^4T_2$ levels split by the low-symmetry crystal field and the $^4A_2$ ground state [4]. The observed g-values given in table 1 are $\sim$1.98, the experimental precision being limited by the ESR linewidths. In consequence, it is difficult to estimate the energies of the $^4T_2$ excited levels from using the g-values determined from the ESR.

The fine-structure parameters are also determined by the energy separations of the $^4T_2$ levels from the ground state and are

$$b_2^0 \equiv D = -2\lambda^2\left(\frac{2}{\Delta_0} - \frac{1}{\Delta_{+1}} - \frac{1}{\Delta_{-1}}\right) \tag{2}$$

$$b_2^2 \equiv 3E = 6\lambda^2\left(\frac{1}{\Delta_{+1}} - \frac{1}{\Delta_{-1}}\right). \tag{3}$$

The measured values (b_2^0, b_2^2) for the D and E spectra are found to be (650×10^{-4} cm^{-1}, -300×10^{-4} cm^{-1}) and (1300×10^{-4} cm^{-1}, -1100×10^{-4} cm^{-1}), respectively. The zero-field splitting ($2\sqrt{(b_2^0)^2 + (b_2^2)^2/3} \simeq 2b_2^0$) of the $^4A_2$ ground state has been estimated to be $\sim 2500 \times 10^{-4}$ cm^{-1} from the fluorescence line narrowing of Cr^{3+} in CYA [1]. The value of b_2^0 is coincident with that obtained from the ESR result. The energy separation $|\Delta_{-1} - \Delta_{+1}|$ ($\sim$2600 cm^{-1}) estimated using the values of the g-shift (0.02), b_2^2, and equation (3) seems to be large because of the large uncertainty of b_2^2. The large separation shows that the contribution of the non-octahedral component of the distortion is dominant.

4.2. Odd-parity distortion

In tetragonal symmetry, the polarization of the $^4A_2 \to {}^4T_2$, $^4T_1$ transitions is induced by the z-component of T_{1u} such that $A_\sigma{:}A_\pi = 1{:}0$ [2]. If the octahedron has trigonal symmetry (the distortion being parallel to the $\langle 111\rangle$ direction of the cubic corners), there are eight equivalent sites. In this case, the polarization is given by the sum over eight sites, resulting in the intensity being isotropic. The observed polarizations of the $^4A_2 \to {}^4T_2$ and $^4A_2 \to {}^4T_1$ absorption bands are $A_\sigma{:}A_\pi \simeq 1{:}3$ and 1:1.5, respectively. This experimental result suggests that the symmetry of the Cr^{3+} complexes is neither tetragonal nor trigonal, but orthorhombic or monoclinic.

The symmetry of the Cr^{3+} complexes determined by the ESR results is orthorhombic as shown in table 1. The principal ξ-, η-, and ζ-axes of the A and B lines are parallel to $\langle 001\rangle$, $\langle 1\bar{1}0\rangle$, and $\langle 110\rangle$. The principal ζ-axes of the D and E spectra are bent away from the $\langle 001\rangle$ direction towards $\langle 111\rangle$ by $\sim 7^\circ$ and $\sim 20^\circ$, respectively.

First, consider the polarization of the $^4A_2 \to {}^4T_2$ transition for the ordered configurations in figure 9(a). The principal ζ-axis is parallel to $\langle 110\rangle$ and that of an equivalent complex is parallel to $\langle 1\bar{1}0\rangle$. If the principal ζ-axis is assumed to be parallel to the direction of an odd-parity distortion, the polarizations for the complexes with $\boldsymbol{\zeta} \parallel \langle 110\rangle$ and $\langle 1\bar{1}0\rangle$ are calculated to be $A_{\langle 001\rangle}{:}A_{\langle 1\bar{1}0\rangle} = 1{:}1$ and $A_{\langle 001\rangle}{:}A_{\langle 110\rangle} = 1{:}1$, respectively. In consequence, the average of the polarization for two equivalent complexes is calculated to be $A_\sigma{:}A_\pi = 1{:}2$, which is very close to the observed ratio.

Next, we calculate the polarization for the disordered complexes, assuming that there are eight equivalent orthorhombic distorted complexes, the unit vector of the principal axes for one of eight complexes being defined as $\boldsymbol{e}_\xi = ((1/\sqrt{2})\cos\alpha, (1/\sqrt{2})\cos\alpha, -\sin\alpha)$, $\boldsymbol{e}_\eta = (\bar{1}/\sqrt{2}, 1/\sqrt{2}, 0)$, and $\boldsymbol{e}_\zeta = ((1/\sqrt{2})\sin\alpha, (1/\sqrt{2})\sin\alpha, \cos\alpha)$. When the E-vector of the radiation is in the ac-plane it is defined as $\boldsymbol{E} = E_0(\sin\theta, 0, \cos\theta)$, where θ is defined as the angle between the E-vector and the c-axis. The polarization obtained by the summing of the contributions from eight equivalent complexes expressed as a function of θ is

$$A(\theta) = (4\sin^2\alpha + 2(1 - 3\sin^2\alpha)\sin^2\theta)A_\xi + 2\sin^2\theta A_\eta + (4\cos^2\alpha + 2(1 - 3\cos^2\alpha)\sin^2\theta)A_\zeta. \quad (4)$$

Assuming that $A_\parallel$ ($=A_\zeta$) and $A_\perp$ ($=A_\xi = A_\eta$), the absorption coefficients, with the E-vector parallel or perpendicular to the principal ζ-axis, are calculated to be

$$A_\pi \equiv A(0) = 4(\sin^2\alpha\, A_\perp + \cos^2\alpha\, A_\parallel) \quad (5)$$

$$A_\sigma \equiv A\left(\frac{\pi}{2}\right) = 2((\cos^2\alpha + 1)A_\perp + \sin^2\alpha\, A_\parallel). \quad (6)$$

The angles α are found to be $\sim 7^\circ$ and $\sim 20^\circ$ from the ESR spectra. The ratio of the polarization obtained using equations (5) and (6) and the parameters $A_\parallel/A_\perp = 3.1$ and 3.8 for the different angles 7° and 20° fits the observed ratio $A_\pi : A_\sigma = 3:1$ very well. In principle, the transition probabilities $A_\parallel$ and $A_\perp$ can be calculated using the wavefunctions of the $^4T_2$ excited state and the $^4A_2$ ground state. However, it is difficult to determine the wavefunctions of $^4T_2$ using only the polarization results.

The R_1-line fluorescence is due to the $^2E \rightarrow {}^4A_2$ transition, which is spin and parity forbidden. The spin-forbidden transition is allowed through the mixing of the $^4T_2$ excited state by spin–orbit interaction. The $^4T_2$ excited state includes an odd-parity wavefunction created by a T_{1u} odd-parity distortion, as discussed above. In consequence, the polarization of the R_1-line fluorescence is very similar to that of the $^4A_2 \rightarrow {}^4T_2$ absorption band.

5. Conclusions

The ordered and disordered configurations of Cr^{3+} in CYA including the second- and third-nearest-neighbouring Ca^{2+}/Y^{3+} ions have been discussed in terms of the ESR spectra and polarization of the optical spectra. The ESR results indicate that there are two kinds of Cr^{3+}-ion complex. Both display orthorhombic symmetry. They differ in that for ordered complexes the principal axes of the ESR spectra are parallel to the mutually perpendicular axes. For the disordered complexes there is an angular rotation of the ζ-axis away from the c-axis of the crystal. The polarizations of the optical spectra calculated for the orthorhombic Cr^{3+} complexes fit the observed data very well. The results of the ESR and polarization spectroscopy provide evidence of the ordered or disordered structures of the neighbourhood of Cr^{3+} ions in CYA.

Acknowledgments

This work was supported by a Grant-in-Aid (07650049) for Scientific Research from the Ministry of Education, Science and Culture and by Joint Research Projects of the Japan Society for the Promotion of Science and the British Council/Royal Society. At Strathclyde the spectroscopic studies of laser materials, of which this work forms a part, are supported by grants from the EPSRC.

References

[1] Yamaga M, Macfarlane P I, Holliday K, Henderson B, Kodama N and Inoue Y 1996 *J. Phys.: Condens. Matter* **8** 3487
[2] Yamaga M, Henderson B and O'Donnell K P 1990 *J. Lumin.* **46** 397

[3] Shannon R D, Oswald R A, Parise J B, Chai B H T, Byszowski P, Pajaczowska A and Sobolewski A 1992 *J. Solid State Chem.* **98** 90
[4] Abragam A and Bleaney B 1970 *Electron Paramagnetic Resonance of Transition Ions* (Oxford: Clarendon) chs 3, 7
[5] Pilbrow J R 1990 *Transition Ion Electron Paramagnetic Resonance* (Oxford: Clarendon) ch 3